

Knockdown of polypyrimidine tract binding protein facilitates motor function recovery after spinal cord injury

Ri-Yun Yang¹, Rui Chai², Jing-Ying Pan¹, Jing-Yin Bao³, Pan-Hui Xia³, Yan-Kai Wang³, Ying Chen¹, Yi Li¹, Jian Wu¹, Gang Chen^{2,3,4,*}

<https://doi.org/10.4103/1673-5374.346463>

Date of submission: December 10, 2021

Date of decision: February 28, 2022

Date of acceptance: April 26, 2022

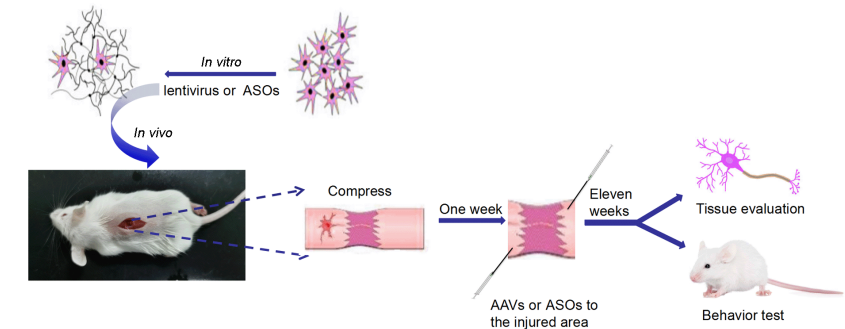
Date of web publication: June 2, 2022

From the Contents

Introduction	396
Methods	397
Results	398
Discussion	399

Graphical Abstract

Knockdown of PTB induces reprogramming of spinal astrocytes into motoneuron-like cells *in vitro* and improves motor function recovery after SCI



Abstract

After spinal cord injury (SCI), a fibroblast- and microglia-mediated fibrotic scar is formed in the lesion core, and a glial scar is formed around the fibrotic scar as a result of the activation and proliferation of astrocytes. Simultaneously, a large number of neurons are lost in the injured area. Regulating the dense glial scar and replenishing neurons in the injured area are essential for SCI repair. Polypyrimidine tract binding protein (PTB), known as an RNA-binding protein, plays a key role in neurogenesis. Here, we utilized short hairpin RNAs (shRNAs) and antisense oligonucleotides (ASOs) to knock down PTB expression. We found that reactive spinal astrocytes from mice were directly reprogrammed into motoneuron-like cells by PTB downregulation *in vitro*. In a mouse model of compression-induced SCI, adeno-associated viral shRNA-mediated PTB knockdown replenished motoneuron-like cells around the injured area. Basso Mouse Scale scores and forced swim, inclined plate, cold allodynia, and hot plate tests showed that PTB knockdown promoted motor function recovery in mice but did not improve sensory perception after SCI. Furthermore, ASO-mediated PTB knockdown improved motor function restoration by not only replenishing motoneuron-like cells around the injured area but also by modestly reducing the density of the glial scar without disrupting its overall structure. Together, these findings suggest that PTB knockdown may be a promising therapeutic strategy to promote motor function recovery during spinal cord repair.

Key Words: antisense oligonucleotides; astrocytes; glial scar; motoneuron-like cells; motor function; neurogenesis; neuron-like cells; polypyrimidine tract binding protein; short hairpin RNAs; spinal cord repair

Introduction

Spinal cord injury (SCI) is a devastating central nervous system injury that often results in paralysis below the injury site (Sofroniew, 2018; Fouad et al., 2021). After SCI, fibroblasts and microglia form fibrotic scars that fill the lesion core. Simultaneously, astrocytes rapidly activate and proliferate, which results in the formation of a dense glial scar around the lesion core. An increasing number of studies have confirmed that the glial scar has dual effects on SCI repair (Yang et al., 2020a). Favorable effects include alleviating further development of inflammatory responses, limiting the spread of fibrotic scars, and forming astrocytic bridges that contribute to axonal regeneration (Anderson et al., 2016; Sofroniew, 2018). However, the glial scar is also regarded as a physical barrier that hinders axons from regenerating through the lesion site and serves as a chemical barrier because of the secretion of molecules that suppress neural regeneration (Li et al., 2020; Escartin et al., 2021). Therefore, the dual role of glial scars makes SCI repair difficult. Our previous study confirmed that 2 weeks was a suitable time point for manipulating the glial scar after SCI (Yang et al., 2020b). In SCI repair, this time point may alleviate the detrimental effects of the glial scar while supporting its favorable effects. During and after SCI, impaired neurons are lost because

of necrosis or apoptosis, and the remaining damaged neurons have little regenerative capacity (O'Shea et al., 2017). These adverse factors coordinate with each other and, ultimately, complicate the SCI repair process. To date, there are no effective approaches for facilitating nerve regeneration and motor function restoration after SCI.

Direct conversion of somatic cells is a promising strategy for clinical use in regenerative medicine. Astrocytes are widely distributed throughout the spinal cord and have high plasticity (Yu et al., 2020). Reactive astrogliosis occurs after SCI, and reactive astrocytes express high levels of the neural stem cell marker nestin and display some characteristics of neural progenitor cells (Liddel and Barres, 2017). Some studies (Su et al., 2014; Puls et al., 2020; Yang et al., 2020b; Liu et al., 2021) have shown that overexpression of neural transcription factors (TFs) can directly reprogram spinal astrocytes into diverse neuronal phenotypes both *in vitro* and *in vivo*. However, these studies mainly used glutamatergic, GABAergic, or mature neurons (Su et al., 2014; Puls et al., 2020; Yang et al., 2020b; Liu et al., 2021). Moreover, these approaches showed limited roles in motor function restoration. Therefore, the strategy for gaining more motor neurons and allowing effective restoration of motor function after SCI requires further investigation.

¹Department of Histology and Embryology, Medical School of Nantong University, Nantong, Jiangsu Province, China; ²Key Laboratory of Neuroregeneration of Jiangsu Province and the Ministry of Education, Co-innovation Center of Neuroregeneration, Nantong University, Nantong, Jiangsu Province, China; ³Center for Basic Medical Research, Medical School of Nantong University, Nantong, Jiangsu Province, China; ⁴Department of Anesthesiology, Affiliated Hospital of Nantong University, Nantong, Jiangsu Province, China

*Correspondence to: Gang Chen, MD, PhD, chengang6626@ntu.edu.cn.
<https://orcid.org/0000-0003-3669-5687> (Gang Chen)

Funding: The study was supported by the National Natural Science Foundation of China, Nos. 82101455 (to RYY), 31872773 (to GC), 82001168 (to JYP); the Key Research and Development Program (Social Development) of Jiangsu Province, No. BE2020667 (to GC); the Foundation of Jiangsu Province "333 Project High-level Talents", No. BRA2020076 (to GC); the Nantong Civic Science and Technology Project of China, No. JC2020028 (to RYY); the Natural Science Research of Jiangsu Higher Education Institutions of China, No. 19KJB310012 (to RYY) and Priority Academic Program Development of Jiangsu Higher Education Institutions (PAPD).

How to cite this article: Yang RY, Chai R, Pan JY, Bao JY, Xia PH, Wang YK, Chen Y, Li Y, Wu J, Chen G (2023) Knockdown of polypyrimidine tract binding protein facilitates motor function recovery after spinal cord injury. *Neural Regen Res* 18(2):396-403.

Poly pyrimidine tract binding protein (PTB, also known as PTBP1), encoded by the *Ptbp1* gene in mice, is an important RNA-binding protein that widely participates in RNA metabolism (Xue et al., 2009). PTB can regulate tau exon 10 inclusion or skipping that leads to neuronal vulnerability (Roussarie et al., 2020). Moreover, PTB plays a key role in neuronal induction. During neurogenesis, the expression level of PTB is naturally decreased (Hu et al., 2018). Studies have demonstrated that knockdown of PTB was able to directly reprogram multiple cell types into neurons or neuron-like cells, including primary mouse embryonic fibroblasts (MEFs), HeLa cells, mouse neural progenitor cells (N2A), human embryonic carcinoma stem cells (NT2), and human retinal epithelial cells (ARPE19) (Xue et al., 2009, 2013). Furthermore, PTB silencing can reprogram midbrain astrocytes into functional dopaminergic (DA) neurons *in vitro*, replenish DA neurons located in the midbrain *in vivo*, and effectively reverse the locomotor phenotype of a mouse model of Parkinson's disease (Qian et al., 2020). In addition, retinal ganglion cells, which are replenished by down-regulation of PTB, promote the recovery of visual responses in mice with retinal injury (Zhou et al., 2020). Maimon et al. (Maimon et al., 2021) confirmed that downregulation of PTB by an antisense oligonucleotide (ASO) significantly reprogrammed astrocytes into neurons *in vitro*. Treatment with a PTB-ASO generated neurons that integrated into the hippocampal circuit and ameliorated the behavioral deficits in aging mice (Maimon et al., 2021).

The above studies show that suppression of PTB expression is a powerful strategy for treating various disorders caused by neuronal loss. However, the function of PTB knockdown in SCI repair has not yet been explored. In this study, short hairpin RNAs (shRNAs) and ASOs were used to knock down the expression of PTB to determine its role both *in vitro* in primary murine reactive spinal astrocytes and *in vivo* using a mouse model of compression-induced SCI.

Methods

ASOs and viral vectors

ASOs were produced by RIBOBIO Biotechnologies (Guangzhou, China). The sequence of the mouse *Ptbp1* ASO (PTB-ASO) was 5'-GGG TGA AGA TCC TGT TCA ATA-3'. The Cy3 fluorochrome was linked to the 5' end of the ASO.

The shRNA sequence targeting mouse *Ptbp1* (shPTB) was 5'-GGG TGA AGA TCC TGT TCA ATA-3'. To construct the lentiviral vector, shPTB was subcloned into the pClenti-GFAP-shRNA (NC)-CMV-EGFP-WPRE vector (OBIO Biotechnologies, Shanghai, China).

To construct adeno-associated virus (AAV) vectors, the same sequence of shPTB was inserted into the pAAV-GFAP-EGFP-MIR155 vector to construct pAAV-GFAP-EGFP-shPTB-MIR155 (Genechem Co., Ltd.; Shanghai, China) (Additional Figure 1). Empty vector was used as a control (shCtrl), and the final viral product titers were as follows: lentivirus-shCtrl, pClenti-GFAP-shRNA(NC)-CMV-EGFP-WPRE (1.31×10^9 transduction units (TU)/mL); lentivirus-shPTB, pClenti-GFAP-shRNA(*Ptbp1*)-CMV-EGFP-WPRE (4.09×10^8 TU/mL); AAV-shCtrl, pAAV-GFAP-EGFP-MIR155 (1.75×10^{13} viral genomes (VG)/mL); and AAV-shPTB, pAAV-GFAP-EGFP-shRNA(*Ptbp1*)-MIR155 (2.71×10^{12} VG/mL).

Primary murine spinal astrocyte culture and activation

All animal experiments were approved by the Institutional Animal Ethics Committee of Nantong University (approval No. S20201015-402) on October 15, 2020. All experiments were designed and reported according to the Animal Research: Reporting of *In Vivo* Experiments (ARRIVE) guidelines (Percie du Sert et al., 2020). Primary murine astrocytes were prepared from the spinal cords of 1–2-day-old Institute of Cancer Research (ICR) mice (Animal Center of Nantong University; Nantong, China; license No. SYXK (Su) 2017-0046) and cultured as described previously (Gao et al., 2016). Neonatal mice were euthanized with carbon dioxide (CO₂). The concentration of CO₂ was continuously increased until respiratory and cardiac arrest occurred, and then a normal supply of oxygen was provided. The CO₂ fill rate was 30–70%, which guaranteed that the mice achieved loss of consciousness before causing pain. The intervention time for CO₂ was 50 minutes (Shomer et al., 2020). Then, mice were placed in 75% ethyl alcohol for 5 minutes. The spinal cords of the mice were separated on ice. The dissociated spinal cords were mechanically minced on ice after removal of the meninges and blood vessels. Tissue was digested using 0.25% trypsin-ethylenediaminetetraacetic acid (Beyotime; Shanghai, China) solution in a 37°C incubator for 15 minutes. The cell suspension was dispersed and immediately filtered through a 100-µm pore membrane (Merck; Darmstadt, Germany). The cells were centrifuged at 157 × *g* for 5 minutes and resuspended in Dulbecco's modified Eagle medium/F12 (DMEM/F12; Gibco; Grand Island, NY, USA) containing 10% fetal bovine serum (Sigma-Aldrich) and 1% penicillin/streptomycin (Gibco). The mixed cells were added to a T-75 flask at a density of 1.0×10^6 cells/mL and maintained in an incubator at 37 °C and 5% CO₂. The conditioned culture medium was replaced every 3 days. After 7 days, primary microglial cells were removed by shaking at 40 × *g* for 16 hours. Primary astrocytes were passaged twice and used for further studies. Lipopolysaccharide (500 ng/mL) was applied for 24 hours to induce astrocyte activation (Agalave et al., 2020).

Reactive astrocyte reprogramming *in vitro*

To induce reprogramming *in vitro*, reactive spinal astrocytes from mice were resuspended in DMEM/F12 medium containing 10% fetal bovine serum and lentivirus-shPTB. The mixture of cells and lentivirus was plated in 6-well cell culture plates (four 12-mm poly-L-lysine-coated glass coverslips/well, 20,000 cells/well). The next day, the medium was changed to induction medium,

which consisted of equal volumes of DMEM/F12 and neurobasal medium (Gibco) supplemented with sodium selenite (30 nM; Sigma-Aldrich), insulin (25 µg/mL; AbMole, USA), putrescine (100 nM; APExBIO; Houston, TX, USA), progesterone (20 nM; Sigma-Aldrich), 2% fetal bovine serum, 0.4% B-27™ (Gibco), SB431542 (10 µM; Sigma-Aldrich), ChIR99021 (1 µM; Sigma-Aldrich), dibutyl-cyclic adenosine monophosphate (1 mM; APExBIO), neurotrophin 3, and 10 ng/mL each of ciliary neurotrophic factor, brain-derived neurotrophic factor, and glial cell-derived neurotrophic factor (Peprotech; Rocky Hill, NJ, USA). One-half volume of the medium was replaced every 3 days.

To determine the function of the PTB-ASOs *in vitro*, primary spinal cord astrocytes were seeded into 6-well culture plates as described above (20,000 cells/well). The following day, PTB-ASOs or control ASOs (75 pmol/well) were transfected using Lipofectamine RNAiMAX (Invitrogen; Carlsbad, CA, USA). The medium was replaced with induction medium after 48 hours for further transdifferentiation.

SCI mouse model

Eight-week-old female ICR mice (specific pathogen-free grade, 23–28 g, Animal Center of Nantong University; license No. SYXK [Su] 2017-0046) were anesthetized throughout the surgery with isoflurane (1–1.5%, flow rate: 200 mL/minute) in oxygenized air supplied by a standard small animal anesthesia device (RWD; Shenzhen, China). SCI leads to urine retention in mice, and male mice are more likely to suffer from urethritis and die than female mice. In addition, the experimental period was up to 12 weeks in this study. Considering the survival rate of mice after SCI, female mice were selected (Wu et al., 2021).

The spinal cord was exposed by a T9–T10 laminectomy. A complete compression injury was induced for 10 seconds by bilateral compression with No. 5 Dumont forceps (Fine Science Tools, Foster City, CA, USA) (Anderson et al., 2018). The overlying muscle was closed with sutures. Wound clips were utilized to close the skin incision. The SCI mice were randomly divided into four groups: AAV-shCtrl, AAV-shPTB, Control ASO, and PTB-ASO groups, each of which included 25 mice.

AAV and ASO injection

AAVs or ASOs may require several days to take effect *in vivo*, and 2 weeks after SCI was considered an appropriate time point to manipulate the glial scar (Yang et al., 2020b). Therefore, we performed injections 7 days after SCI. AAV-shCtrl was diluted to the same titer as AAV-shPTB (2.71×10^{12} VG/mL) with phosphate-buffered saline (PBS). AAVs were injected at two oblique points on opposite sides of the lesion site (1.0 mm caudal and rostral to the lesion core at approximately 45°, 1.5 µL per injection) utilizing a 10 µL microsyringe with a 33G needle (Hamilton, Basel, Switzerland). The method for injecting ASOs (1 µg/µL, 1.0 µL per injection) was the same as that for injecting AAVs. At 12 weeks after SCI, mice were deeply anesthetized with intraperitoneally administered ethyl carbamate (Sinopharm Chemical Reagent Co. Ltd., Shanghai, China) and then sacrificed. The spinal cords of the mice were collected.

Western blot analysis and quantitative reverse transcription-polymerase chain reaction

For measuring protein expression levels of PTB following PTB silencing in reactive spinal astrocytes, the reprogrammed cells were lysed in cell lysis buffer containing cComplete™ Protease Inhibitor Cocktail (Roche, Mannheim, Germany). After quantification, equivalent amounts of reprogrammed cell protein from each treatment group were resolved by sodium dodecyl sulfate-polyacrylamide gel electrophoresis. Proteins were then transferred to a polyvinylidene difluoride membrane (Merck Millipore, Billerica, MA, USA). After blocking with 5% skim milk (Beyotime), the membrane was incubated with specific primary antibodies for 18 hours at 4°C. Then, after three washes with Tris-buffered saline containing Tween-20, the membrane was incubated with the corresponding secondary antibody for 2 hours at 25°C. Immunoreactions were visualized with a chemiluminescent substrate (Thermo Fisher Scientific, Waltham, MA, USA) and a fully automated ChemiDoc system (Tanon, Shanghai, China). The primary antibodies and dilutions were as follows: rabbit anti-glyceraldehyde 3-phosphate dehydrogenase (GAPDH; 1:1000; Beyotime, Cat# AF 1186) and rabbit anti-PTB (1:1000; ABclonal, Wuhan, China, Cat# A3487, RRID: AB_2863069). The secondary antibody was horseradish peroxidase-conjugated goat anti-rabbit IgG (1:5000; Thermo Fisher Scientific, Cat# 31466, RRID: AB_10960844). ImageJ 1.47v software (National Institutes of Health, Bethesda, MD, USA) (Schneider et al., 2012) was used to quantify the protein band signals.

Total RNA from reprogrammed cells or spinal cord was extracted using TRI reagent (Sigma-Aldrich). The RNA was reverse transcribed to complementary deoxyribonucleic acid (cDNA) using a reverse transcription kit (Thermo Fisher Scientific). Polymerase chain reaction (PCR) was performed using a QuantiNova SYBR Green PCR Kit (Qiagen, Duesseldorf, Germany) and Bio-Rad CFX96 Real-Time PCR instrument (Hercules, CA, USA). The quantitative reverse transcription PCR mixture (20 µL) contained 6 µL RNase-free water, 10 µL SYBR Green, 1 µL forward primer, 1 µL reverse primer, and 2 µL cDNA. Reaction conditions were: pre-denaturation at 95°C for 2 minutes followed by 40 cycles of denaturation at 95°C for 5 seconds and annealing at 60°C for 10 seconds. The relative expression of target genes was normalized to *Gapdh*. The primer sequences are listed in Table 1.

Table 1 | Primers used for quantitative reverse transcription-polymerase chain reaction

Gene	Sequence	Product length (bp)
<i>Ptbp1</i>	Forward: 5'-AGA GGA GGC TGC CAA CAC TA-3'	286
	Reverse: 5'-GTC CAG GGT CAC TGG GTA GA-3'	
<i>Caspase-3</i>	Forward: 5'-GAG CTT GGA ACG GTA CGC TAA-3'	118
	Reverse: 5'-GAG TCC ACT GAC TTC CTG CC-3'	
<i>Caspase-9</i>	Forward: 5'-GAG CTT CGA GAA CTA CCG CA-3'	84
	Reverse: 5'-GTA TTC CCG CGA TCC CCT G-3'	
<i>Gfap</i>	Forward: 5'-CGG AGA CGC ATC ACC TCT G-3'	126
	Reverse: 5'-AGG GAG TGG AGG AGT CAT TCG-3'	
<i>Gapdh</i>	Forward: 5'-GGT GAA GGT CCG TGT GAA CCG-3'	143
	Reverse: 5'-TCA TAC TGG AAC ATG TAG ACC-3'	

Gapdh: Glyceraldehyde-3-phosphate dehydrogenase; Gfap: glial fibrillary acidic protein; Ptbp1: polypyrimidine tract-binding protein.

Immunocytochemistry

To measure astrocyte transdifferentiation *in vitro*, reprogrammed cells were collected after 3 and 4 weeks of lentivirus-shPTB-mediated PTB knockdown or 5 weeks of PTB ASO-mediated PTB knockdown and fixed with 4% paraformaldehyde for 10 minutes. Cells were permeabilized in PBS containing 1% Triton X-100 for 15 minutes and then washed three times with PBS. Cells were blocked with 3% bovine serum albumin in PBS for 30 minutes and incubated with specific primary antibodies diluted in PBS containing 3% bovine serum albumin for 16 hours at 4°C. The primary antibodies included mouse anti-microtubule-associated protein 2 (MAP2; 1:600; Abcam, Cambridge, MA, USA, Cat# ab11268, RRID: AB_297886), goat anti-green fluorescent protein (GFP; 1:1000; Abcam, Cat# ab5450, RRID: AB_304897), rabbit anti-choline acetyltransferase (ChAT; 1:400; Abcam, Cat# ab181023, RRID: AB_2687983), and goat anti-glial fibrillary acidic protein (GFAP; 1:600; Abcam, Cat# ab53554, RRID: AB_880202). After washing three times with PBS, reprogrammed cells were incubated for 2 hours at room temperature with the following secondary antibodies: Alexa Fluor 488-labeled donkey anti-goat IgG (1:1000; Thermo Fisher Scientific, Cat# A11055, RRID: AB_2534102), Alexa Fluor 488-labeled donkey anti-rabbit IgG (1:1000; Thermo Fisher Scientific, Cat# A21206, RRID: AB_2535792), Alexa Fluor 568-labeled donkey anti-mouse IgG (1:1000; Thermo Fisher Scientific, Cat# A10037, RRID: AB_2534013), or Alexa Fluor 647-labeled donkey anti-rabbit IgG (1:1000; Thermo Fisher Scientific, Cat# A31573, RRID: AB_2536183). Nuclei were labeled with Hoechst 33342 (Beyotime) by incubation for 15 minutes at 37°C. Images were acquired using a confocal microscope (Leica, Wetzlar, Germany). MAP2⁺, GFP⁺, ChAT⁺, GFAP⁺, and Hoechst⁺ cells were counted.

Immunohistochemistry

To measure the localization of shPTB delivered by AAV in the spinal cord of mice, spinal cord staining was conducted 1 week after injection. To explore the role of PTB knockdown *in vivo*, spinal cord staining was conducted 12 weeks after SCI. Mice were anesthetized with isoflurane and perfused transcardially with 0.9% NaCl followed by 4% paraformaldehyde. The T9–T11 vertebrae of the spinal cord were excised and postfixed with 4% paraformaldehyde for 10 hours at 4°C and then incubated for 1 week in 30% sucrose at 4°C. Spinal cord sections (16 µm) were prepared using a freezing microtome (Leica). The spinal cord sections were blocked for 1 hour at 37°C in PBS containing 0.3% Triton X-100 and 3% bovine serum albumin. The steps were similar to those used for staining reprogrammed cells on coverslips as described above. The spinal cord sections were incubated with specific primary antibodies diluted in PBS containing 3% bovine serum albumin for 16 hours at 4°C. The following primary antibodies were used: goat anti-GFAP (1:600, Abcam, Cat# ab53554), mouse anti-GFAP (1:600, Abcam, Cat# ab279289), mouse anti-NeuN (1:600, Abcam Cat# ab104224, RRID: AB_10711040), rabbit anti-ChAT (1:400, Abcam, Cat# ab181023), mouse anti-MAP2 (1:600, Abcam, Cat# ab11268), goat anti-GFP (1:1000; Abcam, Cat# ab5450), and mouse anti-FoxJ1 (1:400, Abcam, Cat# ab220028). After washing three times with PBS, the sections were incubated for 2 hours at 25°C with Alexa Fluor 488-labeled donkey anti-goat IgG (1:1000), Alexa Fluor 568-labeled donkey anti-mouse IgG (1:1000), or Alexa Fluor 647-labeled donkey anti-rabbit IgG (1:1000) as described above.

Slices across the spinal cord were sampled at eight slice intervals and subjected to immunofluorescent staining for ChAT, NeuN, MAP2, GFP, and GFAP. Stereological methods were used to count the total number of cells of a given type (Abercrombie, 1946), and the formula utilized was previously described (Qian et al., 2020). The percentages of NeuN⁺, MAP2⁺, and ChAT⁺ neurons among GFP⁺ cells were quantified at 12 weeks after SCI. The immunofluorescence density of the GFAP signal in the glial scar area around the lesion core (Yang et al., 2020b) was determined quantitatively using ImageJ software.

Terminal deoxynucleotidyl transferase dUTP nick-end labeling

To explore the effect of PTB knockdown on apoptosis, sections across the spinal cord were prepared as described above, fixed with 4% paraformaldehyde for 60 minutes, and washed two times with PBS. Sections were permeabilized in PBS containing 0.5% Triton X-100 for 5 minutes at room temperature. After washing two times with PBS, the sections were incubated with the terminal deoxynucleotidyl transferase dUTP nick-end labeling (TUNEL) detection liquid (Beyotime) for 1 hour at 37°C. Nuclei were labeled with

Hoechst 33342 by incubation for 15 minutes at 37°C. Images were acquired with a confocal microscope, and the numbers of TUNEL⁺ cells were counted. The percentages were calculated as the number of TUNEL⁺ cells divided by the total number of Hoechst⁺ cells.

Behavioral experiments

Motor recovery was measured at 1 week post-SCI and then weekly for 12 weeks post-SCI.

Basso Mouse Scale score

The motor function of SCI mice was evaluated using the Basso Mouse Scale (BMS) scoring system (Huang et al., 2020). Two trained evaluators scored the mice in a double-blinded manner. Mice were evaluated for at least 5 minutes after scouting the open field environment for 20 minutes. The score was from 0 to 9. A higher score represented improved function of both hindlimbs.

Forced swim test

The swimming ability of each SCI mouse was evaluated using the forced swim test. A rectangular plexiglass container (42 cm × 30 cm × 35 cm) filled with water was used for the test with a water depth of approximately 18 cm and temperature at approximately 23°C (Yang et al., 2020b). The swim test was performed for 1 minute each time and repeated three times at 15 minutes intervals. An HD camera was utilized to photograph the swimming process. The swing frequency of the hindlimb was determined every 10 seconds. The maximum swing frequency during each minute was measured, and the mean value of three tests was calculated.

Inclined plate test

The muscle strength of both hindlimbs of SCI mice was evaluated using the inclined plate test (Yang et al., 2020b), which consisted of a rectangular plexiglass box (42 cm × 7 cm × 8 cm) with a rough wooden surface at the bottom. When the box was inclined, the mice would slide down from the rough surface because of gravity. We gradually raised the tilt of the box until the mice could no longer maintain position for 5 seconds without sliding down. The recorded result was generated from the maximum height of the top of the box perpendicular to the horizontal plane. The test was repeated three times, and the maximum height was used as the result.

Cold allodynia

The sensory recovery of SCI mice was assessed by the cold allodynia test. Cold allodynia was scored by the acetone solution method (Burton et al., 1999). 50 µL of acetone solution was placed onto the plantar skin surface of the paw through a blunt needle attached to a syringe. The reaction of the mouse was observed within 20 seconds: adiphoria, scored 0; minor response, scored 1; moderate reaction—the hindpaw was lifted but did not touch any surface when sprayed with acetone, scored 2; strong response—the paw was licked, bit, and shaken, scored 3. The test was repeated three times at 15 minute intervals, and the mean value was recorded.

Hot plate test

The hot plate test was used to assess the sensory function of SCI mice (Luszczki and Czuczwar, 2008). Mice were placed in a clear 25 cm × 25 cm chamber with a height of 40 cm. The chamber contained a metal plate, and the surface temperature of the plate was 55 ± 0.5°C. The cumulative time that the mouse lifted its hindpaw from the hot plate and licked the paw within a 30 second interval was calculated. The experiment was repeated three times at 15 minute intervals, and the mean value of the three experiments was calculated.

Statistical analysis

The numbers of repeated samples or mice are listed in the figure legends. Degrees of freedom were used to predetermine sample sizes for the *in vivo* study (Charan and Kantharia, 2013), and sample sizes were estimated according to our previous studies for similar behavioral, immunofluorescence, and TUNEL staining analyses (Yang et al., 2020b). Outcome assessors were blinded to the assignment. All data are presented as the means ± standard error of mean (SEM). All statistical analyses were performed with GraphPad Prism 6.01 software (GraphPad Software, San Diego, CA, USA; www.graphpad.com). The Shapiro-Wilk test was utilized to measure data normality. Western blot, RT-PCR, immunocytochemistry, and immunohistochemistry reactivity were analyzed using two-tailed Student's *t*-tests. Behavioral data were analyzed using repeated measures two-way analysis of variance with Tukey's *post hoc* tests. A value of *P* < 0.05 was considered statistically significant.

Results

ShPTB mediates direct conversion of reactive spinal astrocytes from mice into motoneuron-like cells *in vitro*

Given the demonstrated direct neuronal conversion of cultured mouse cortical astrocytes after shPTB treatment (Qian et al., 2020), we explored whether PTB silencing led to the conversion of reactive mouse spinal astrocytes into motor neurons *in vitro*. In a reactive astrocyte model, we treated primary murine spinal astrocytes with lipopolysaccharide (Additional Figure 2A and B). Next, we transduced reactive spinal astrocytes from mice with a lentiviral vector containing a *Gfap* promoter driving the expression of an shRNA against mouse *Ptbp1*. When astrocytes were transduced with this vector for 2 days, shPTB significantly downregulated both the protein expression of PTB and mRNA expression of *Ptbp1* (Figure 1A–C). At 2 weeks post-reprogramming, shPTB-infected cells showed complex neurite outgrowth, and, by 4 weeks, these cells displayed obvious neuronal morphology, whereas cells transduced with the

shCtrl displayed an astrocyte-like flattened and polygonal morphology (Figure 1D). Three weeks after transduction, approximately 41% of shPTB-transduced GFP⁺ cells demonstrated positive staining for the neuronal marker MAP2 (Figure 1E and F). At 4 weeks post-conversion, the percentage of GFP⁺/MAP2⁺ cells was approximately 58%, and approximately 12% of GFP⁺ cells exhibited expression of the motor neuron marker ChAT (Figure 1G and H). In contrast, cells transduced with the shCtrl lentiviral vector exhibited positive staining only for GFP (Figure 1E and G). These data demonstrate that reactive spinal astrocytes can be reprogrammed into motoneuron-like cells by PTB silencing *in vitro*.

PTB silencing replenishes motoneuron-like cells around the injured area after SCI

SCI induces the loss of a large number of neurons in the injured area (Anderson et al., 2016). To determine whether PTB silencing replenished neurons, including motor neurons, in an SCI mouse model, we injected AAVs into the oblique opposite sides of the injured spinal area. We used the Gfap promoter to drive shPTB expression. A large number of GFP⁺ cells were colocalized with GFAP⁺ astrocytes 1 week after injection (Figure 2A), whereas the GFP⁺ cells were rarely colocalized with ChAT⁺ motor neurons (Figure 2B). Quantitatively, approximately 75% of GFP⁺ cells were colocalized with GFAP⁺ astrocytes, but no GFP⁺ cells were colocalized with ChAT⁺ motoneurons (Figure 2C). Moreover, the GFP⁺ cells did not colocalize with FoxJ1⁺ neural stem cells (Additional Figure 3A and B). Eleven weeks after AAV-shPTB injection, some GFP⁺ cells were co-labeled with the neuronal marker NeuN or MAP2 around the injured area (Figure 3A and B). Quantitatively, approximately 30% and 29% of GFP⁺ cells were co-labeled with NeuN and MAP2, respectively (Figure 3C). Furthermore, approximately 19% of GFP⁺ cells expressed the motor neuron-specific marker ChAT at 11 weeks after AAV-shPTB injection (Figure 3A–C). At this same time point, neither GFP⁺ neuron-like cells nor GFP⁺ motoneuron-like cells were detected around the injured area after AAV-shCtrl injection (Figure 3A–C). Quantitative analysis of neuronal-like cell and motoneuron-like cell populations around the lesion area showed that the number of NeuN⁺, MAP2⁺, and ChAT⁺ cells were more abundant in the AAV-shPTB group compared with that in the AAV-shCtrl group (Figure 3D). In conclusion, these results reveal that shPTB can replenish motoneuron-like cells around the injured area after SCI.

PTB knockdown facilitates motor function restoration in SCI mice

We determined whether PTB knockdown could promote functional recovery in SCI mice. We used the BMS score and swim test to evaluate motor recovery. A compression SCI was induced in mice, and AAV-shPTB or AAV-shCtrl was injected *in situ* 1 week post-injury (Figure 4). BMS scores were decreased at 1 week post-SCI. At 6–12 weeks post-injury, AAV-shPTB-injected mice showed higher BMS scores than AAV-shCtrl mice (Figure 5A). However, there was no obvious difference between the two groups in the swim test (Figure 5B). AAV-shPTB-injected mice maintained position at a higher height than AAV-shCtrl mice at 12 weeks post-SCI in the inclined plate test (Figure 5C). These results demonstrated improved muscle strength recovery after PTB knockdown. Sensory recovery was assessed by the cold allodynia and hot plate tests. The AAV-shPTB-injected mice did not exhibit any improvement in performance compared with that of AAV-shCtrl-injected mice in either the cold allodynia or hot plate test at 6–12 weeks post-SCI (Figure 5D and E). These findings indicate that AAV-shPTB treatment can improve motor recovery after SCI.

Conversion of spinal astrocytes into motoneuron-like cells *in vitro* after transfection with PTB-ASOs

Given the demonstrated capability of ASOs to degrade their target mRNAs (Bennett et al., 2019; Qian et al., 2020; Maimon et al., 2021), downregulation of PTB by PTB-ASO suggests a clinically feasible strategy. As shown in Figure 6A–C, compared with the control ASO, PTB-ASO transfection markedly reduced PTB protein and *Ttpb1* mRNA expression in astrocytes after 2 days. At 5 weeks post-transfection, we evaluated the morphology of reprogrammed cells and the expression of the mature neuronal marker MAP2 as well as the motor neuron marker ChAT via immunocytochemistry (Figure 6D). Quantitative analysis of MAP2⁺ and ChAT⁺ cells among total Hoechst⁺ cells showed that approximately 64% of the reprogrammed cells exhibited neurite outgrowth and expressed MAP2, and approximately 14% of the reprogrammed cells exhibited positive ChAT staining (Figure 6D and E). These results suggest that PTB-ASO significantly induced the conversion of reactive spinal astrocytes into motoneuron-like cells *in vitro*.

PTB-ASOs reduce the density of glial scars and replenished motoneuron-like cells in SCI mice

As previously described, the glial scar has a dual role in SCI repair. Some studies have suggested that moderate reduction in the glial scar can play a positive role in functional recovery after SCI (Rodriguez et al., 2014; Hesp et al., 2018; Yang et al., 2020b). We determined the effects of PTB ASOs on glial scar density by GFAP staining of the injured spinal cord. As shown in Figure 7A, at 12 weeks after SCI, control ASO-injected mice showed typical glial scar morphology with interdigitating astrocytes that displayed a considerable number of parallel processes. PTB-ASO-injected mice also exhibited integrated glial scar structures, which were different from the exhaustive ablation of glial scars in some previous reports. In PTB ASO-injected mice, glial scar-derived astrocytes were loosely distributed with fewer parallel processes (Figure 7A). Quantitative analysis of the immunofluorescent intensity of GFAP around the lesion area revealed a moderate decrease in the density of glial scars in PTB ASO-injected mice compared with that in control ASO-injected mice (Figure 7B).

SCI results in irreversible loss of neurons in the injured area, and the regenerative capacity of the damaged neurons is limited (Sofroniew, 2018).

To explore the potential beneficial function of the PTB-ASO in SCI mice, we determined whether injection of the PTB-ASO into the injured spinal cord replenished neurons, including motor neurons. This strategy may be helpful for promoting functional recovery after massive SCI-associated loss of neurons in the lesion area. We found that control ASO-injected mice exhibited an obvious decrease in NeuN⁺ and ChAT⁺ cells in the region proximal to the lesion area compared with the distal region at 12 weeks after SCI (Figure 7A). In contrast, PTB-ASO-injected mice retained many NeuN⁺ and ChAT⁺ cells in the region proximal to the lesion at a level similar to that observed in the distal site (Figure 7A). Quantitatively, the number of NeuN⁺ and ChAT⁺ cells in the region proximal to the lesion area was greater in PTB-ASO-injected mice compared with that in control ASO-injected mice (Figure 7C). TUNEL staining was utilized to detect cell apoptosis around the lesion area at 12 weeks post-SCI. We found that the number of TUNEL⁺ cells around the lesion area was lower in PTB-ASO-injected mice than in control ASO-injected mice (Figure 8A and B). Furthermore, quantitative RT-PCR analysis of mRNA from injured spinal tissue exhibited lower expression levels of the apoptotic markers caspase-3 and caspase-9 in PTB-ASO-injected mice compared with those in control ASO-injected mice (Figure 8C). These findings revealed that the PTB-ASO reduced glial scar density without disrupting its overall structure, replenished motoneuron-like cells around the SCI lesion area, and decreased apoptotic cell death in the injured spinal cord.

PTB-ASOs promote motor function recovery in SCI mice

The function of the PTB-ASO was further evaluated by behavioral tests in SCI mice. Strikingly, compared with the control ASO, the PTB-ASO enhanced motor function recovery from 5–12 weeks post-SCI as determined by BMS scores and swim tests (Figure 9A and B). The PTB-ASO-treated mice reached a higher height than control ASO-treated mice in the inclined plate test at 12 weeks post-SCI (Figure 9C). Compared with control ASO-treated mice, PTB ASO-treated mice tended to use their lower limbs and displayed greater muscle strength after SCI. In the sensory system, cold- and heat-induced sensory responses were not different between the PTB-ASO-treated and control ASO-treated mice from 6–12 weeks post-injury (Figure 9D and E). These results demonstrated that PTB-ASOs promoted motor function recovery in SCI model mice.

Discussion

SCI is a serious neurological disorder with the pathological characteristics of fibrotic fibroblast-mediated cavitation, astrogliosis-mediated glial scar formation around the cavity, and loss of major motor neurons, which ultimately causes failure of axonal regeneration in the injured area. At present, research on SCI repair mainly focuses on inhibiting astroglial-fibrous scar formation, supplementing neurons, and improving nerve regeneration. However, many therapeutic approaches, such as signal transducer and activator of transcription 3 knockout, leads to the exhaustive ablation of the glial scar, which results in poor functional recovery after SCI (Anderson et al., 2016; Sofroniew, 2018; Gu et al., 2019). Moreover, many approaches that replenish neurons around the injured area do not achieve satisfactory functional recovery after SCI (Huang et al., 2020; Yang et al., 2020b). Thus, the identification of efficacious therapeutic approaches for SCI is an extremely urgent need. As mentioned earlier, PTB can regulate the inclusion or skipping of tau exon 10, which leads to neuronal vulnerability (Roussarie et al., 2020). In addition, PTB has an important effect on neuronal induction, and its expression level is naturally reduced during neurogenesis (Hu et al., 2018). Our current study is the first to explore the function of silencing PTB in SCI.

As previously described, the glial scar has dual effects on SCI repair. An appropriate method to treat the glial scar needs to be discovered to alleviate the adverse effects of the scar while supporting its favorable role in SCI repair. Our previous studies confirmed that 2 weeks post-SCI is a suitable time point for manipulating the glial scar because the formation of the scar is almost complete by this time after injury (Yang et al., 2020b). Because gene therapies may take additional days to stably alter gene expression, we postponed the *in situ* injection for 7 days after SCI. Thus, the effects of gene therapy began around 2 weeks after SCI, which coincided precisely with the appropriate time point to manipulate the glial scar. In our study, we found that PTB knockdown modestly reduced the density of the glial scar and maintained the structure of the scar after SCI in contrast to exhaustive scar ablation.

Somatic cell reprogramming is an alternative to cell replacement therapy and shows great potential in SCI repair. As some previous studies have shown, spinal astrocytes can be reprogrammed into neurons. Our team previously revealed that the SOX2 TF can reprogram glial scar-forming astrocytes into neurons in a mouse model of SCI (Yang et al., 2020b). More recently, activation of the endogenous neuron-related genes *Ngn2* and *Isl1* was shown to reprogram astrocytes into motor neurons in the spinal cord of adult mice (Zhou et al., 2021). The proneural ASCL1 TF reprograms spinal astrocytes into neurons *in vitro* (Kempf et al., 2021). The *Ngn2* gene reprograms spinal astrocytes into neurons both *in vitro* and *in vivo* (Kempf et al., 2021; Liu et al., 2021). The proneural OCT4 and KLF4 TFs can facilitate motor recovery in a mouse model of SCI, and combinations of TFs can reprogram astrocytes into neural stem cell-like cells *in vitro* (Huang et al., 2020). *Neurod1* induces resident astrocytes to undergo neuronal reprogramming after SCI (Puls et al., 2020). In SCI, the combination of SOX2 and valproic acid can reprogram astrocytes to neurons (Su et al., 2014). However, to date, only *Ngn2* and *Isl1* have been found to reprogram spinal astrocytes into motor neurons, while most other strategies result in astrocyte-derived glutamatergic, GABAergic, or mature neurons. Thus, the identification of new key TFs or genes involved in motor neuron replenishment is expected to be a new breakthrough.

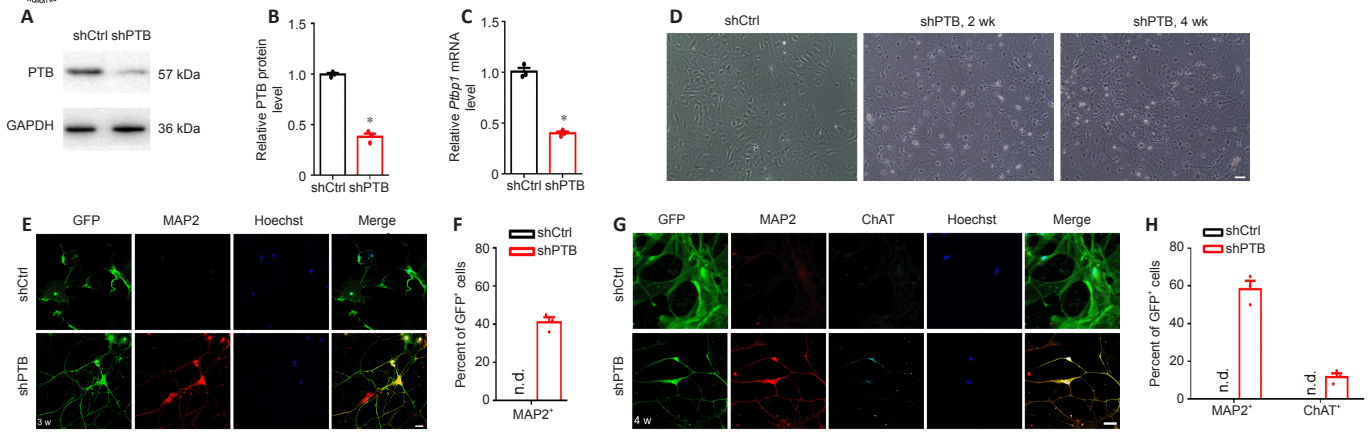


Figure 1 | Direct reprogramming of primary murine reactive spinal astrocytes into motoneuron-like cells by PTB knockdown *in vitro*. (A) Western blot bands and (B) quantification of the protein expression levels of PTB following PTB silencing with short hairpin (sh)PTB RNA in reactive mouse spinal astrocytes for 2 days. The results were normalized to the shCtrl (shCtrl) group. (C) *Ptbp1* mRNA levels after PTB knockdown for 2 days. The results were normalized to the shCtrl group. (D) Representative photographs of the morphological changes following PTB silencing for 2 and 4 weeks. After PTB silencing for 2 weeks, shPTB-infected cells showed complex neurite outgrowth, and these cells displayed obvious neuronal morphology by 4 weeks, whereas cells transfected with shCtrl displayed an astrocyte-like flattened and polygonal morphology. Scale bar: 40 μ m. (E) Reactive mouse spinal astrocytes were immunostained for the neuronal marker MAP2 (red, Alexa Fluor 568) after PTB knockdown for 3 weeks. There were some shPTB-transduced GFP⁺ (green, Alexa Fluor 488) cells that stained positive for MAP2, whereas no shCtrl-transduced GFP⁺ cells were positive for MAP2. Scale bar: 40 μ m. (F) Quantification of the number of MAP2⁺ cells among transduced GFP⁺ cells at 3 weeks. (G) Reprogrammed motoneuron-like cell morphology and expression of ChAT (cyan, Alexa Fluor 647) after PTB silencing for 4 weeks. There were some shPTB-transduced GFP⁺ (green, Alexa Fluor 488) cells that stained positive for ChAT, whereas no shCtrl-transduced GFP⁺ cells stained positive for ChAT. Scale bar: 40 μ m. (H) Quantification of the number of MAP2⁺ cells and ChAT⁺ cells among transduced GFP⁺ cells at 4 weeks. Data are shown as the means \pm SEM. The experiments were repeated three times. **P* < 0.05, vs. shCtrl (two-tailed Student's *t*-test). ChAT: choline acetyltransferase; GAPDH: glyceraldehyde-3-phosphate dehydrogenase; GFP: green fluorescent protein; MAP2: microtubule-associated protein 2; n.d.: not detected; PTB: polypyrimidine tract-binding protein; Ptbp1: polypyrimidine tract-binding protein; w: weeks.

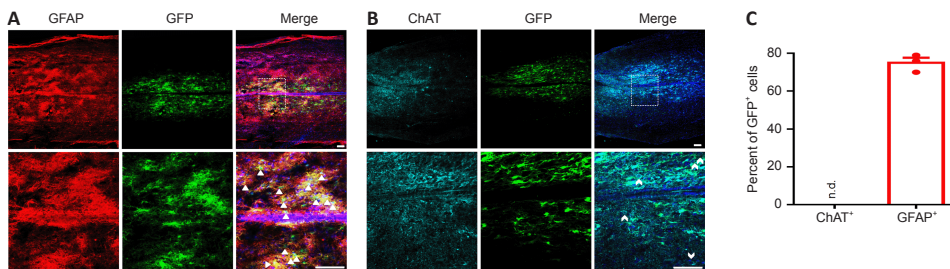


Figure 2 | Localization of shPTB delivered by AAV in the spinal cord of mice. At 1 week post-injection; immunohistochemical staining showed that GFP⁺ (green, Alexa Fluor 488) cells colocalized with GFAP⁺ (red, Alexa Fluor 568) astrocytes (A) but not with ChAT⁺ (cyan, Alexa Fluor 647) motor neurons (B). The lower panels are magnifications of the white dashed box areas in the upper panels to improve clarity. The arrowheads in (A) indicate representative co-labeled spinal astrocytes, and the swallowtail arrowheads in (B) denote endogenous motor neurons (*n* = 3 mice, four sections per mouse). Scale bars: 50 μ m. (C) Quantitative analysis of the percentage of GFAP⁺ and ChAT⁺ cells colocalizing with GFP⁺ cells. The data are presented as the means \pm SEM (*n* = 3 mice/group) and were analyzed by two-tailed Student's *t*-test. AAV: Adeno-associated virus; ChAT: choline acetyltransferase; GFAP: glial fibrillary acidic protein; GFP: green fluorescent protein; n.d.: not detected; PTB: polypyrimidine tract-binding protein.

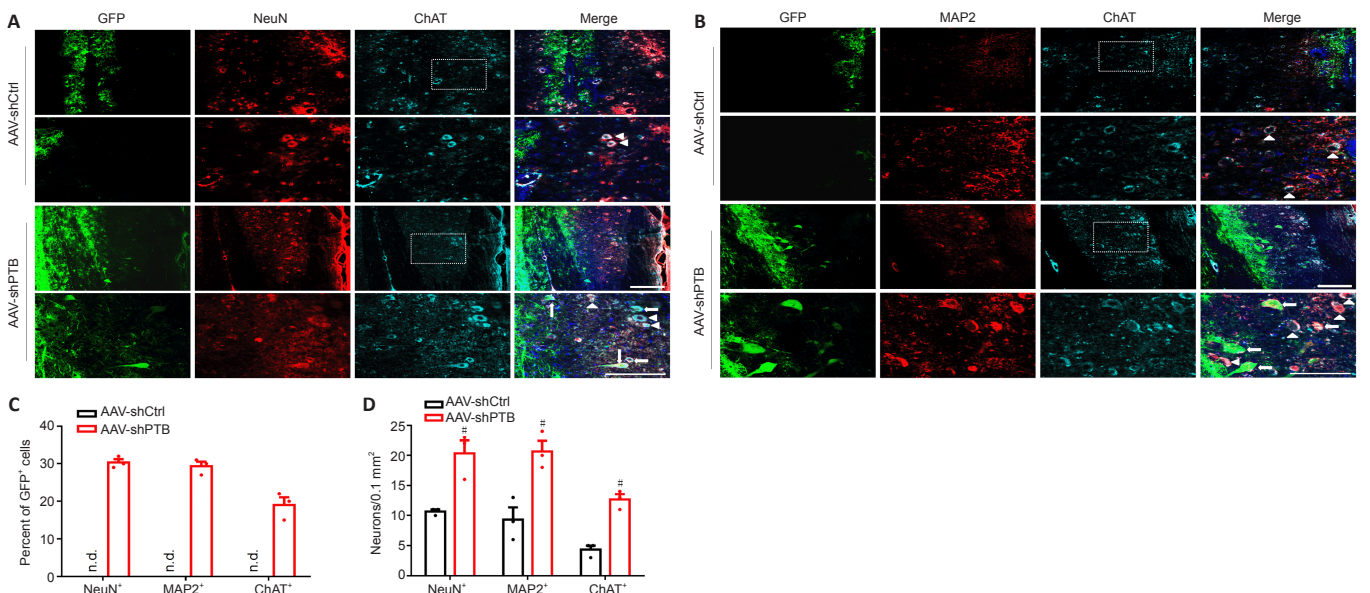


Figure 3 | PTB knockdown replenished motoneuron-like cells around the injured area after SCI in mice. (A) Longitudinal sections at 12 weeks post-SCI. In the AAV-shPTB group, some of the GFP⁺ (green, Alexa Fluor 488) cells were colocalized with NeuN⁺ (red, Alexa Fluor 568) and ChAT⁺ (cyan, Alexa Fluor 647) cells. The arrows show representative supplementary motoneuron-like cells, and the arrowheads indicate representative endogenous motor neurons. In the AAV-shCtrl group, there were no co-labeled GFP⁺/NeuN⁺ cells or GFP⁺/ChAT⁺ cells (*n* = 3 mice, four sections per mouse). Scale bars: 200 μ m. In each group, the lower panels are magnifications of the white dashed box areas in the upper panels to improve clarity. (B) Replenished neuron-like cells (GFP⁺ [green, Alexa Fluor 488] and MAP2⁺ [red, Alexa Fluor 568]) and motoneuron-like cells (GFP⁺/ChAT⁺ [cyan, Alexa Fluor 647]) were detected in the AAV-shPTB group 12 weeks after SCI. The arrows denote representative replenished motoneuron-like cells, and the arrowheads indicate representative endogenous motor neurons. There were no GFP⁺/MAP2⁺ or GFP⁺/ChAT⁺ cells in the AAV-shCtrl group (*n* = 3 mice, four sections per mouse). Scale bars: 200 μ m. (C) Quantitative analysis of the percentage of NeuN⁺, MAP2⁺, and ChAT⁺ cells among the GFP⁺ cells (*n* = 3 mice). (D) Quantitative analysis of total NeuN⁺, MAP2⁺, and ChAT⁺ cells around the injured spinal cord areas in the AAV-shCtrl and AAV-shPTB mouse groups. The data are shown as the means \pm SEM (*n* = 3 mice/group). #*P* < 0.05, vs. AAV-shCtrl (two-tailed Student's *t*-test). AAV: Adeno-associated virus; ChAT: choline acetyltransferase; GFP: green fluorescent protein; MAP2: microtubule-associated protein 2; PTB: polypyrimidine tract-binding protein; SCI: spinal cord injury.

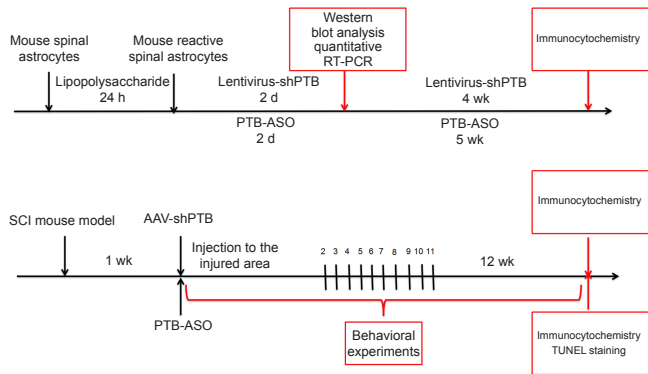


Figure 4 | The experimental timelines.

AAV: Adeno-associated virus; ASO: antisense oligonucleotide; PTB: polypyrimidine tract-binding protein; RT-PCR: reverse transcription-polymerase chain reaction; SCI: spinal cord injury; TUNEL: TdT-mediated dUTP Nick-End Labeling.

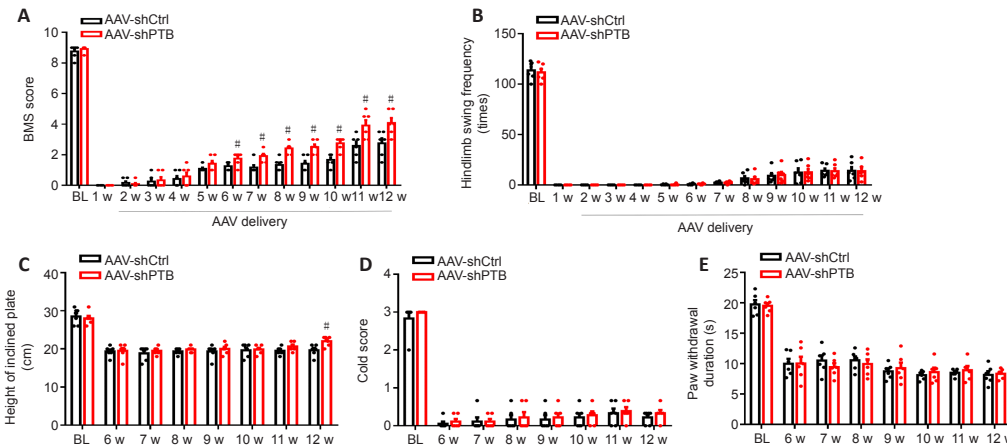


Figure 5 | PTB knockdown facilitated motor function recovery after SCI.

(A) BMS scores. Motor function recovery was better in mice with AAV-shPTB-mediated PTB knockdown from 6 to 12 weeks after SCI than in mice that received the AAV-shCtrl. (B) The swim, (C) inclined plate, (D) cold allodynia, and (E) hot plate tests. No obvious differences were observed in the swim, cold allodynia, and hot plate tests between the AAV-shCtrl and AAV-shPTB groups. The inclined plate test showed that AAV-shPTB-injected mice maintained their position at a greater height than AAV-shCtrl mice at 12 weeks post-SCI. The data are shown as the means \pm SEM ($n = 6$ mice/group). $\#P < 0.05$, vs. AAV-shCtrl (repeated measures two-way analysis of variance followed by Tukey's *post hoc* test). AAV: Adeno-associated virus; BL: baseline; BMS: Basso Mouse Scale; PTB: polypyrimidine tract-binding protein; SCI: spinal cord injury; w: week(s).

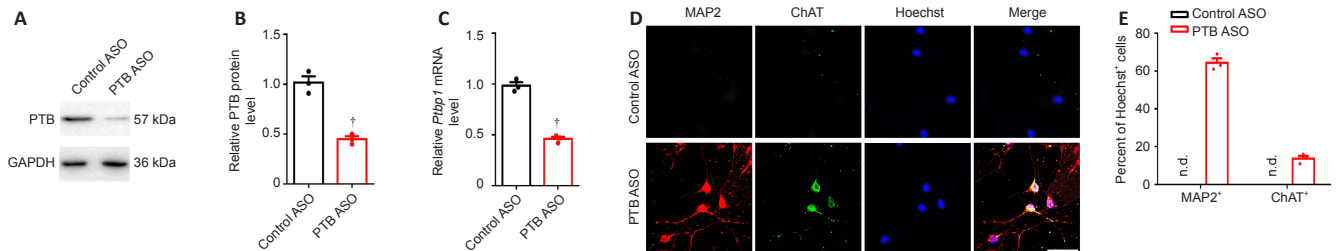


Figure 6 | The PTB-ASO mediated the reprogramming of murine reactive spinal astrocytes to motoneuron-like neurons *in vitro*.

The protein expression levels of PTB were measured by (A) western blot analysis after PTB-ASOs were transfected into murine reactive spinal astrocytes for 2 days. (B) Quantification of PTB protein. The results were normalized to the Control ASO group. (C) The mRNA expression levels of *Ptpb1* following PTB silencing for 2 days. The results were normalized to the Control ASO group. (D) Representative images of the expression of ChAT (green, Alexa Fluor 488) by immunocytochemical staining after PTB-ASO-mediated PTB knockdown for 5 weeks. In the PTB-ASO group, MAP2⁺ (red, Alexa Fluor 568) cells stained positive for ChAT (green, Alexa Fluor 488), but there were no MAP2⁺ and ChAT⁺ cells in the Control ASO group. Scale bar: 40 μ m. (E) Quantitatively, the efficiencies of neuron-like and motoneuron-like cell reprogramming were calculated based on the percentages of MAP2⁺ and ChAT⁺ cells among total Hoechst⁺ cells. The experiments were repeated three times. The data are shown as the means \pm SEM. $\dagger P < 0.05$, vs. control ASO (two-tailed Student's *t*-test). ASO: Antisense oligonucleotide; ChAT: choline acetyltransferase; GAPDH: glyceraldehyde-3-phosphate dehydrogenase; MAP2: microtubule-associated protein 2; n.d.: not detected; PTB: polypyrimidine tract-binding protein; Ptpb1: polypyrimidine tract-binding protein.

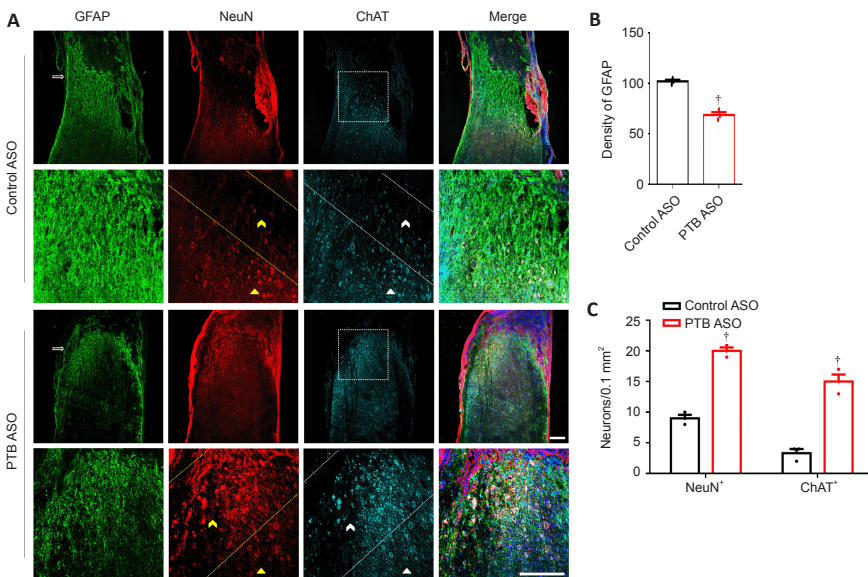


Figure 7 | The PTB-ASO reduces the density of the glial scar and replenishes motoneuron-like cells around the spinal cord lesion.

(A) At 12 weeks post-SCI, the GFAP (green, Alexa Fluor 488) fluorescence intensity was lower and the number of NeuN⁺ (red, Alexa Fluor 568) and ChAT⁺ (cyan, Alexa Fluor 647) cells was much greater around the lesion area in PTB-ASO-injected mice than in the Control ASO group. The arrows indicate the glial scar area. The yellow swallowtail arrowheads and lines surrounding the area denote the NeuN⁺ cells in the region proximal to the lesion area. The white swallowtail arrowheads and lines surrounding the area denote the ChAT⁺ cells around the damaged area. The yellow arrowheads and lines surrounding the area indicate NeuN⁺ cells in the region distal to the damaged area. The white arrowheads and lines surrounding the area denote ChAT⁺ cells in the region distal to the damaged area ($n = 3$ mice; four sections per mouse). Scale bars: 200 μ m. In each group, the lower panels are magnifications of the white dashed box areas in the upper panels to improve clarity. (B) Quantitative analysis of the fluorescence intensity of GFAP in the glial scar area. (C) Quantitative analysis of the numbers of NeuN⁺ and ChAT⁺ cells per 0.1 mm² in the region proximal to the lesion area. The data are shown as the means \pm SEM ($n = 3$ mice/group). $\dagger P < 0.05$, vs. control ASO (two-tailed Student's *t*-test). ASO: Antisense oligonucleotide; ChAT: choline acetyltransferase; GFAP: glial fibrillary acidic protein; PTB: polypyrimidine tract-binding protein; SCI: spinal cord injury.

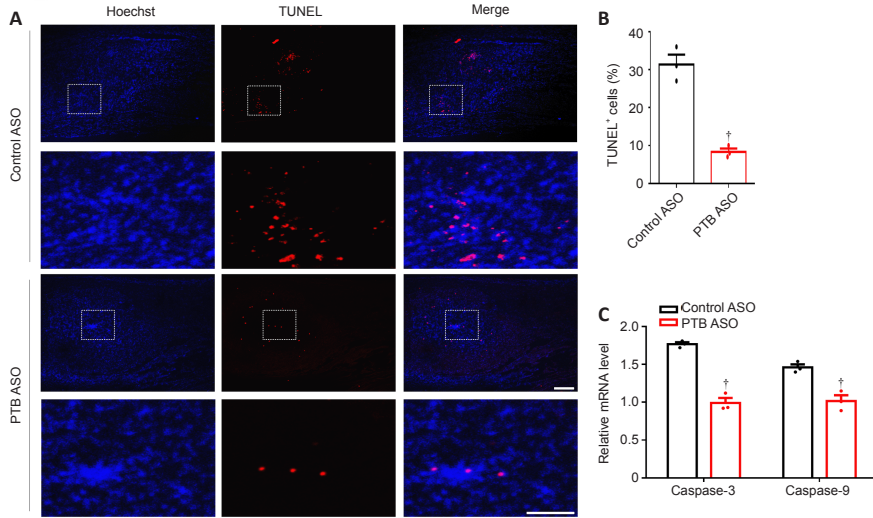


Figure 8 | The PTB-ASO prevented apoptosis of injured spinal cord cells.

(A) Twelve weeks after SCI, PTB-ASO-injected mice had fewer TUNEL⁺ cells than control ASO-injected mice around the injured area ($n = 3$ mice; four sections per mouse). Scale bars: 200 μm . In each group, the lower panels are magnifications of the white dashed box areas in the upper panels to improve clarity. (B) Quantitative analysis of the percentage of TUNEL⁺ cells. (C) The mRNA expression levels of caspase-3 and caspase-9 in the injured spinal cord of PTB-ASO-injected mice were lower than those of control ASO-injected mice. The data are shown as the means \pm SEM ($n = 3$ mice/group). $\dagger P < 0.05$, vs. control ASO (two-tailed Student's t -test). ASO: Antisense oligonucleotide; PTB: polypyrimidine tract-binding protein; SCI: spinal cord injury; TUNEL: TdT-mediated dUTP nick-end labeling.

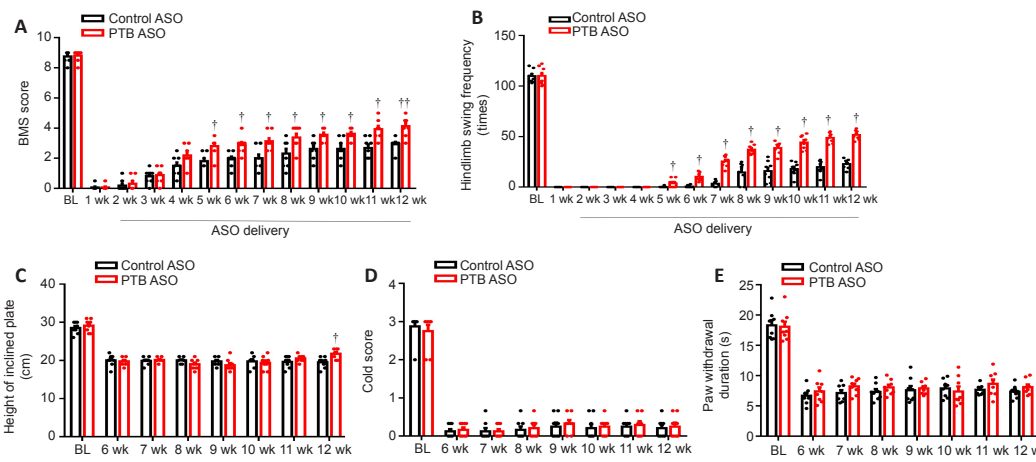


Figure 9 | PTB-ASOs facilitates motor function recovery in SCI mice.

After PTB-ASO injection in mice, motor function recovery following SCI was better than that in the control ASO group from 5 to 12 weeks. Motor function recovery was assessed using the BMS score (A) and swim test (B) weekly after SCI. (C) In the inclined plate test, PTB-ASO-treated mice reached a higher height than control ASO-treated mice at twelve weeks post-SCI. (D) The cold allodynia and (E) hot plate tests were used to detect sensory function recovery and indicated that there were no marked differences between the control ASO and PTB-ASO groups. The data are shown as the means \pm SEM ($n = 8$ mice/group). $\dagger P < 0.05$, $\dagger\dagger P < 0.01$, vs. control ASO (repeated measures two-way analysis of variance followed by Tukey's *post hoc* test). ASO: Antisense oligonucleotide; BL: baseline; PTB: polypyrimidine tract-binding protein; SCI: spinal cord injury.

PTB participates in the regulation of RNAs involved in neural differentiation. Neurons have a positive RE1-silencing transcription factor (REST)/miR-124 signaling loop related to neural induction. In this loop, miR-124 efficiently inhibits the expression of non-neural genes (including REST). However, in non-neural cells, PTB expression induces a negative feedback REST/miR-124 loop in which REST downregulates the expression of many neural-specific TFs and miR-124 (Xue et al., 2013; Hu et al., 2018). Thus, the regulation of PTB plays a key role in the cell fate decision of the neuronal lineage. Various cells, including MEFs, N2A, NT2, and ARPE19 cells, can be gradually reprogrammed into functional neurons via activation of the REST/miR-124 loop induced by PTB knockdown (Xue et al., 2013). Notably, astrocytes have the same regulated signaling loop for neuronal maturation as neurons; thus, PTB knockdown alone leads to the activation of a positive REST/miR-124 feedback loop (Qian et al., 2020). This characteristic increases the feasibility of one-step reprogramming of astrocytes into neurons by reducing PTB expression. Qian et al. (2020) confirmed that a single one-step strategy that suppressed PTB significantly induced reprogramming of midbrain astrocytes into functional DA neurons *in vitro*. In a mouse model of Parkinson's disease, after PTB knockdown for 3 months, this strategy improved motor function by not only replenishing DA neurons but also by rebuilding the striatal dopamine circuit (Qian et al., 2020). Maimon et al. (2021) demonstrated that ASO-mediated PTB knockdown reprogrammed astrocytes into neurons *in vitro*. In aging mice, this PTB-ASO replenished neurons in the brain and modified behavioral dysfunction (Maimon et al., 2021). Moreover, many studies have reported that the region-specific status of astrocytes strongly affects the cell conversion process. Astrocytes from different regions have different transcriptional and proteomic environments and, potentially, region-specific neural TFs that lead to conversion into different subtype-specific neurons (Mattugini et al., 2019; Herrero-Navarro et al., 2021; Kempf et al., 2021). The property of regionalization is maintained during astrocyte-to-neuron conversion both *in vitro* and *in vivo*. Because the spinal cord contains an abundance of motor neurons, we successfully reprogrammed reactive spinal astrocytes into motoneuron-like cells through PTB knockdown *in vitro*. Interestingly, a challenge has recently been raised in the field (Wang et al., 2021), where PTB knockdown failed to reprogram brain astrocytes into neurons *in vivo* over a relatively short period of time, and endogenous neurons were the source of the presumed astrocyte-derived neurons. Some scholars believe that astrocytic reprogramming is a long and gradual developmental process

that requires a relatively long time to be observed *in vivo*, and the conversion rate may be related to the appropriate virus concentration and type. In our mouse model of compression-induced SCI, we found that PTB silencing for approximately 3 months not only reduced the density of the glial scar without disrupting its overall structure but also replenished motoneuron-like cells around the injured area and decreased apoptotic cell death in the injured spinal cord, which ultimately led to the promotion of motor function recovery. Based on the present studies (Qian et al., 2020; Wang et al., 2021), we speculate that the supplemented motoneuron-like cells may either be induced by astrocytic reprogramming, originate from endogenous neurons because of the neuronal protective effect of PTB knockdown, or are derived from PTB knockdown-mediated residual neural stem cell differentiation. Thus, the origin of the supplemented motoneuron-like cells in SCI mice after PTB silencing requires confirmation by further studies.

In this study, we used AAVs and ASOs as gene therapeutics to target Ptbp1. We are the first to use an shPTB and a PTB-ASO to reprogram spinal astrocytes into motoneuron-like cells *in vitro*. In our study, AAV-mediated delivery of shPTB and ASO-mediated knockdown of PTB were shown for the first time to replenish motoneuron-like cells around the injured area after SCI. Moreover, after SCI, the PTB-ASO replenished the motoneuron-like cells in the lesion area, decreased apoptotic cell death in the injured spinal cord, and modestly reduced the density of glial scar without destroying its overall structure. The use of AAVs as viral vectors for gene delivery is clinically feasible because of their minimal immunogenicity, wealth of engineered tissue-specific serotypes, and minimal insertion mutagenesis rate (Wu et al., 2006). Recently, some AAV-mediated clinical gene therapeutic approaches have been verified, such as GlaxoSmithKline's severe combined immunodeficiency therapy (Naldini, 2015). AAVs are a better choice than other viral vectors for shRNA delivery *in vivo*. Recombinant AAVs provide rapid and steady expression within 1 week (Mason et al., 2010). The formation of glial scars almost completely ceased 2 weeks post-SCI, and, thus, 1 week post-SCI is a better time point for injection of AAVs into the injured area. AAV-mediated shRNA expression can be sustained for months or even years *in vivo* with low toxicity (Aguar et al., 2017). Moreover, in 2016, an ASO gene technology for spinal muscular atrophy therapy was approved by the U.S. Food and Drug Administration (Tosolini and Sleight, 2017), which contributes to gene therapy of motor neurons. ASOs are synthetic chemically modified single strands of 15–25 nucleotides that efficiently reduce the expression

level of target genes by binding to specific sequences of pre-mRNA or mRNA (Amado and Davidson, 2021). When injected into the central nervous system, ASOs can be distributed widely (Rigo et al., 2014; Tosolini and Sleigh, 2017). Moreover, ASOs have drug-like features and are easy to regulate (Kordasiewicz et al., 2012), and manufacturing of ASOs is simple. All of these properties make ASOs suitable for therapy of some medical diseases. However, ASOs have more off-target effects and cause more inflammatory reactions and toxicity than AAVs (Rao et al., 2009). Although both AAV-mediated shRNA and ASOs are reported to knock down specific genes efficiently, the type of strategy must be carefully selected to improve the therapeutic effect. The determination of efficacy differences between these two strategies for SCI repair will require further investigations.

In summary, we found that PTB knockdown replenished motoneuron-like cells around the injured area, decreased apoptotic cell death in the injured spinal cord, and moderately reduced the density of the glial scar without disrupting its overall structure, thereby facilitating motor function recovery after SCI. In addition, a limitation of this approach was that the functional recovery extended only to improved motor ability but did not include improvement in sensory perception. As a result, further improvements of this therapeutic approach will be required. The serious consequences of SCI are a result of many factors. Future studies should consider strategies for SCI repair from multiple aspects, such as combining PTB knockdown strategies with other engineering techniques, with the aim of further enhancing functional recovery after SCI.

Author contributions: *Study design, and manuscript draft:* GC, RYY; *experiment implementation:* RYY, RC, JYP, JYB, PHX, YKW, YC, YL, JW. All authors contributed to the manuscript revision, read, and approved the final version of the manuscript.

Conflicts of interest: *The authors declare that the research was conducted in the absence of any commercial or financial relationships that could be construed as a potential conflict of interest.*

Availability of data and materials: *All data generated or analyzed during this study are included in this published article and its supplementary information files.*

Open access statement: *This is an open access journal, and articles are distributed under the terms of the Creative Commons AttributionNonCommercial-ShareAlike 4.0 License, which allows others to remix, tweak, and build upon the work non-commercially, as long as appropriate credit is given and the new creations are licensed under the identical terms.*

Open peer reviewer: Lukas Grassner, Trauma Center Murnau, Germany.

Additional files:

Additional Figure 1: *Schematic diagram of pAAV-GFAP-EGFP-MIR155(Ptbp1) (left) and pClenti-GFAP-shRNA(Ptbp1)-CMV-EGFP-WPRE.*

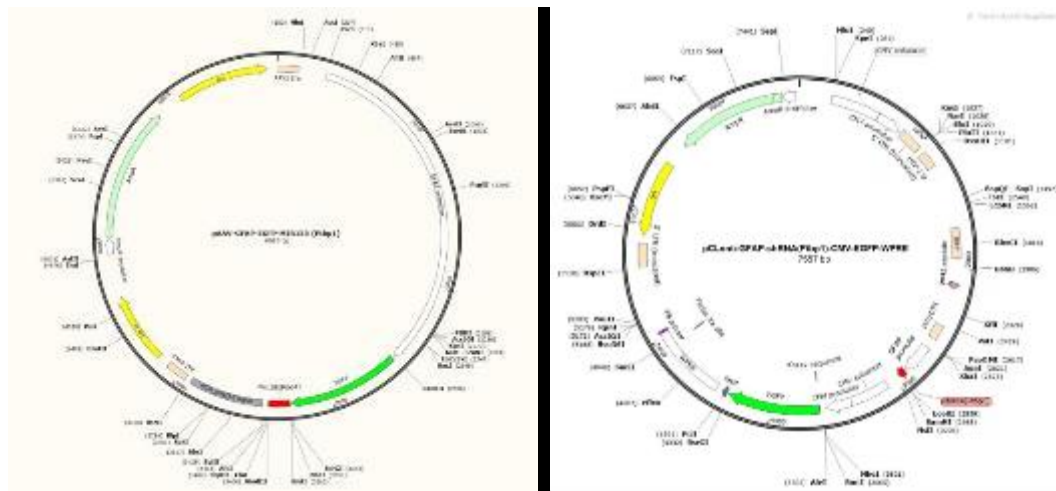
Additional Figure 2: *Establishment of a cell model of mouse reactive spinal astrocytes.*

Additional Figure 3: *Localization of neural stem cells in the injured spinal cord of mice.*

References

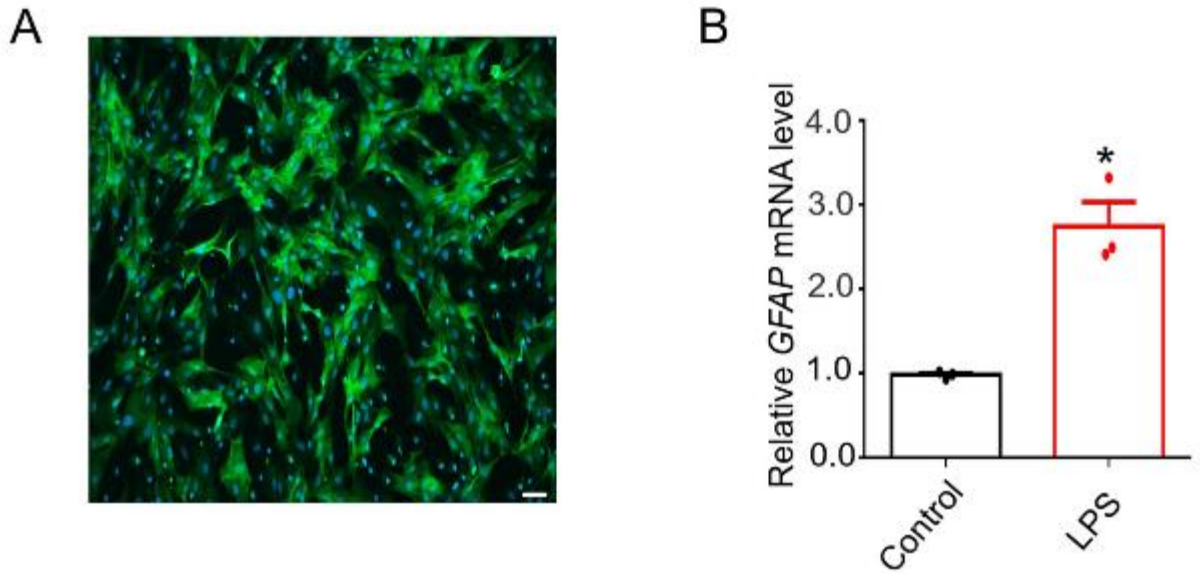
- Abercrombie M (1946) Estimation of nuclear population from microtome sections. *Anat Rec* 94:239-247.
- Agalave NM, Lane BT, Mody PH, Szabo-Pardi TA, Burton MD (2020) Isolation, culture, and downstream characterization of primary microglia and astrocytes from adult rodent brain and spinal cord. *J Neurosci Methods* 340:108742.
- Aguiar S, van der Gaag B, Cortese FAB (2017) RNAi mechanisms in Huntington's disease therapy: siRNA versus shRNA. *Transl Neurodegener* 6:30.
- Amado DA, Davidson BL (2021) Gene therapy for ALS: a review. *Mol Ther* 29:3345-3358.
- Anderson MA, Burda JE, Ren Y, Ao Y, O'Shea TM, Kawaguchi R, Coppola G, Khakh BS, Deming TJ, Sofroniew MV (2016) Astrocyte scar formation aids central nervous system axon regeneration. *Nature* 532:195-200.
- Anderson MA, O'Shea TM, Burda JE, Ao Y, Barlaty SL, Bernstein AM, Kim JH, James ND, Rogers A, Kato B, Wollenberg AL, Kawaguchi R, Coppola G, Wang C, Deming TJ, He Z, Courtine G, Sofroniew MV (2018) Required growth facilitators propel axon regeneration across complete spinal cord injury. *Nature* 561:396-400.
- Bennett CF, Krainer AR, Cleveland DW (2019) Antisense oligonucleotide therapies for neurodegenerative diseases. *Annu Rev Neurosci* 42:385-406.
- Burton AW, Lee DH, Saab C, Chung JM (1999) Preemptive intrathecal ketamine injection produces a long-lasting decrease in neuropathic pain behaviors in a rat model. *Reg Anesth Pain Med* 24:208-213.
- Charan J, Kantharia ND (2013) How to calculate sample size in animal studies? *J Pharmacol Pharmacother* 4:303-306.
- Escartin C, Galea E, Lakatos A, O'Callaghan JP, Petzold GC, Serrano-Pozo A, Steinhäuser C, Volterra A, Carmignoto G, Agarwal A, Allen NJ, Araque A, Barbeito L, Barzilai A, Bergles DE, Bonvento G, Butt AM, Chen WT, Cohen-Salmon M, Cunningham C, et al. (2021) Reactive astrocyte nomenclature, definitions, and future directions. *Nat Neurosci* 24:312-325.
- Fouad K, Popovich PG, Kopp MA, Schwab JM (2021) The neuroanatomical-functional paradox in spinal cord injury. *Nat Rev Neurol* 17:53-62.
- Gao X, Xia J, Munoz FM, Manners MT, Pan R, Meucci O, Dai Y, Hu H (2016) STIMs and Orail1 regulate cytokine production in spinal astrocytes. *J Neuroinflammation* 13:126.
- Gu Y, Cheng X, Huang X, Yuan Y, Qin S, Tan Z, Wang D, Hu X, He C, Su Z (2019) Conditional ablation of reactive astrocytes to dissect their roles in spinal cord injury and repair. *Brain Behav Immun* 80:394-405.
- Herrero-Navarro A, Puche-Aroca L, Moreno-Juan V, Sempere-Ferrández A, Espinosa A, Susin R, Torres-Masjoan L, Leyva-Díaz E, Karow M, Figueres-Oñate M, López-Mascaraque L, López-Atalaya JP, Berninger B, López-Bendito G (2021) Astrocytes and neurons share region-specific transcriptional signatures that confer regional identity to neuronal reprogramming. *Sci Adv* 7:eabe8978.
- Hesp ZC, Yoseph RY, Suzuki R, Jukkola P, Wilson C, Nishiyama A, McTigue DM (2018) Proliferating NG2-cell-dependent angiogenesis and scar formation alter axon growth and functional recovery after spinal cord injury in mice. *J Neurosci* 38:1366-1382.
- Hu J, Qian H, Xue Y, Fu XD (2018) PTB/nPTB: master regulators of neuronal fate in mammals. *Biophys Rep* 4:204-214.
- Huang X, Wang C, Zhou X, Wang J, Xia K, Yang B, Gong Z, Ying L, Yu C, Shi K, Shu J, Cheng F, Han B, Liang C, Li F, Chen Q (2020) Overexpression of the transcription factors OCT4 and KLF4 improves motor function after spinal cord injury. *CNS Neurosci Ther* 26:940-951.
- Kempf J, Knelles K, Hersbach BA, Petrik D, Riedemann T, Bednarova V, Janjic A, Simon-Ebert T, Enard W, Smialowski P, Götz M, Masserdotti G (2021) Heterogeneity of neurons reprogrammed from spinal cord astrocytes by the proneural factors Ascl1 and Neurogenin2. *Cell Rep* 36:109409.
- Kordasiewicz HB, Stanek LM, Wancewicz EV, Mazur C, McAlonis MM, Pytel KA, Artates JW, Weiss A, Cheng SH, Shihabuddin LS, Hung G, Bennett CF, Cleveland DW (2012) Sustained therapeutic reversal of Huntington's disease by transient repression of huntingtin synthesis. *Neuron* 74:1031-1044.
- Li X, Li M, Tian L, Chen J, Liu R, Ning B (2020) Reactive astrogliosis: implications in spinal cord injury progression and therapy. *Oxid Med Cell Longev* 2020:9494352.
- Liddelow SA, Barres BA (2017) Reactive Astrocytes: Production, Function, and Therapeutic Potential. *Immunity* 46:957-967.
- Liu F, Zhang Y, Chen F, Yuan J, Li S, Han S, Lu D, Geng J, Rao Z, Sun L, Xu J, Shi Y, Wang X, Liu Y (2021) Neurog2 directly converts astrocytes into functional neurons in midbrain and spinal cord. *Cell Death Dis* 12:225.
- Luszczki JJ, Czuczwar SJ (2008) Dose-response relationship analysis of vigabatrin doses and their antinociceptive effects in the hot-plate test in mice. *Pharmacol Rep* 60:409-414.
- Maimon R, Chillon-Marinhas C, Snethlage CE, Singhal SM, McAlonis-Downes M, Ling K, Rigo F, Bennett CF, Da Cruz S, Hnasko TS, Muotri AR, Cleveland DW (2021) Therapeutically viable generation of neurons with antisense oligonucleotide suppression of PTB. *Nat Neurosci* 24:1089-1099.
- Mason MR, Ehrhart EM, Eggers R, Pool CW, Hermening S, Huseinovic A, Timmermans E, Blits B, Verhaagen J (2010) Comparison of AAV serotypes for gene delivery to dorsal root ganglion neurons. *Mol Ther* 18:715-724.
- Mattugini N, Bocchi R, Scheuss V, Russo GL, Torper O, Lao CL, Götz M (2019) Inducing different neuronal subtypes from astrocytes in the injured mouse cerebral cortex. *Neuron* 103:1086-1095.e5.
- Naldini L (2015) Gene therapy returns to centre stage. *Nature* 526:351-360.
- O'Shea TM, Burda JE, Sofroniew MV (2017) Cell biology of spinal cord injury and repair. *J Clin Invest* 127:3259-3270.
- Percie du Sert N, Hurst V, Ahluwalia A, Alam S, Avey MT, Baker M, Browne WJ, Clark A, Cuthill IC, Dirnagl U, Emerson M, Garner P, Holgate ST, Howells DW, Karp NA, Lázic SE, Lidster K, MacCallum CJ, Macleod M, Pearl EJ, et al. (2020) The ARRIVE guidelines 2.0: Updated guidelines for reporting animal research. *PLoS Biol* 18:e3000410.
- Puls B, Ding Y, Zhang F, Pan M, Lei Z, Pei Z, Jiang M, Bai Y, Forsyth C, Metzger M, Rana T, Zhang L, Ding X, Keefe M, Cai A, Redilla A, Lai M, He K, Li H, Chen G (2020) Regeneration of functional neurons after spinal cord injury via in situ neurod1-mediated astrocyte-to-neuron conversion. *Front Cell Dev Biol* 8:591883.
- Qian H, Kang X, Hu J, Zhang D, Liang Z, Meng F, Zhang X, Xue Y, Maimon R, Dowdy SF, Devaraj NK, Zhou Z, Mobley WC, Cleveland DW, Fu XD (2020) Reversing a model of Parkinson's disease with in situ converted nigral neurons. *Nature* 582:550-556.
- Rao DD, Vorhies JS, Senzer N, Nemunaitis J (2009) siRNA vs. gRNA: similarities and differences. *Adv Drug Deliv Rev* 61:746-759.
- Rigo F, Chun SJ, Norris DA, Hung G, Lee S, Matson J, Fey RA, Gaus H, Hua Y, Grundy JS, Krainer AR, Henry SP, Bennett CF (2014) Pharmacology of a central nervous system delivered 2'-O-methoxyethyl-modified survival of motor neuron splicing oligonucleotide in mice and nonhuman primates. *J Pharmacol Exp Ther* 350:46-55.
- Rodriguez JP, Coulter M, Miotke J, Meyer RL, Takemaru K, Levine JM (2014) Abrogation of β -catenin signaling in oligodendrocyte precursor cells reduces glial scarring and promotes axon regeneration after CNS injury. *J Neurosci* 34:10285-10297.
- Roussarie JP, Yao V, Rodriguez-Rodriguez P, Oughtred R, Rust J, Plautz Z, Kasturia S, Albornoz C, Wang W, Schmidt EF, Dannenfels R, Tadych A, Brichta L, Barnea-Cramer A, Heintz N, Hof PR, Heiman M, Dolinski K, Flajolet M, Troyanskaya OG, et al. (2020) Selective neuronal vulnerability in Alzheimer's disease: a network-based analysis. *Neuron* 107:821-835.e12.
- Schneider CA, Rasband WS, Eliceiri KW (2012) NIH Image to ImageJ: 25 years of image analysis. *Nat Methods* 9:671-675.
- Shomer NH, Allen-Worthington KH, Hickman DL, Jonnalagadda M, Newsome JT, Slate AR, Valentine H, Williams AM, Wilkinson M (2020) Review of rodent euthanasia methods. *J Am Assoc Lab Anim Sci* 59:242-253.
- Sofroniew MV (2018) Dissecting spinal cord regeneration. *Nature* 557:343-350.
- Su Z, Niu W, Liu ML, Zou Y, Zhang CL (2014) In vivo conversion of astrocytes to neurons in the injured adult spinal cord. *Nat Commun* 5:3338.
- Tosolini AP, Sleigh JN (2017) Motor neuron gene therapy: lessons from spinal muscular atrophy for amyotrophic lateral sclerosis. *Front Mol Neurosci* 10:405.
- Wang LL, Serrano C, Zhong X, Ma S, Zou Y, Zhang CL (2021) Revisiting astrocyte to neuron conversion with lineage tracing in vivo. *Cell* 184:5465-5481.e16.
- Wu J, Lu B, Yang R, Chen Y, Chen X, Li Y (2021) EphB2 knockdown decreases the formation of astroglial-fibrotic scars to promote nerve regeneration after spinal cord injury in rats. *CNS Neurosci Ther* 27:714-724.
- Wu Z, Asokan A, Samulski RJ (2006) Adeno-associated virus serotypes: vector toolkit for human gene therapy. *Mol Ther* 14:316-327.
- Xue Y, Zhou Y, Wu T, Zhu T, Ji X, Kwon YS, Zhang C, Yeo G, Black DL, Sun H, Fu XD, Zhang Y (2009) Genome-wide analysis of PTB-RNA interactions reveals a strategy used by the general splicing repressor to modulate exon inclusion or skipping. *Mol Cell* 36:996-1006.
- Xue Y, Ouyang K, Huang J, Zhou Y, Ouyang H, Li H, Wang G, Wu Q, Wei C, Bi Y, Jiang L, Cai Z, Sun H, Zhang K, Zhang Y, Chen J, Fu XD (2013) Direct conversion of fibroblasts to neurons by reprogramming PTB-regulated microRNA circuits. *Cell* 152:82-96.
- Yang T, Dai Y, Chen G, Cui S (2020a) Dissecting the dual role of the glial scar and scar-forming astrocytes in spinal cord injury. *Front Cell Neurosci* 14:78.
- Yang T, Xing L, Yu W, Cai Y, Cui S, Chen G (2020b) Astrocytic reprogramming combined with rehabilitation strategy improves recovery from spinal cord injury. *FASEB J* 34:15504-15515.
- Yu X, Nagai J, Khakh BS (2020) Improved tools to study astrocytes. *Nat Rev Neurosci* 21:121-138.
- Zhou H, Su J, Hu X, Zhou C, Li H, Chen Z, Xiao Q, Wang B, Wu W, Sun Y, Zhou Y, Tang C, Liu F, Wang L, Feng C, Liu M, Li S, Zhang Y, Xu H, Yao H, et al. (2020) Glia-to-neuron conversion by CRISPR-CasRx alleviates symptoms of neurological disease in mice. *Cell* 181:590-603.e16.
- Zhou M, Tao X, Sui M, Cui M, Liu D, Wang B, Wang T, Zheng Y, Luo J, Mu Y, Wan F, Zhu LQ, Zhang B (2021) Reprogramming astrocytes to motor neurons by activation of endogenous Ngn2 and Isl1. *Stem Cell Reports* 16:1777-1791.

P-Reviewer: Grassner Paduraru L; C-Editor: Zhao M; S-Editors: Yu J, Li CH; L-Editors: Zunino S, Yu J, Song LP; T-Editor: Jia Y



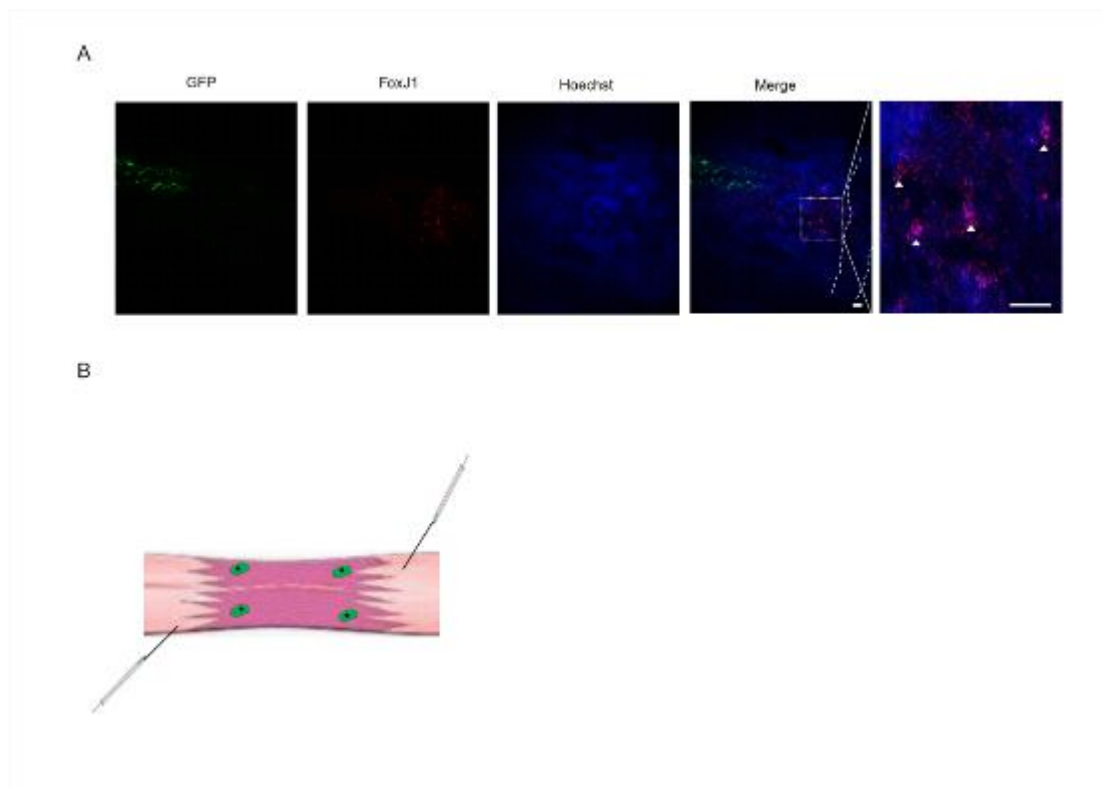
Additional Figure 1 Schematic diagram of pAAV-GFAP-EGFP-MIR155(*Ptbp1*) (left) and pClenti-GFAP-shRNA(*Ptbp1*)-CMV-EGFP-WPRE.

Created with SnapGene® software (from Insightful Science; available at snapgene.com).



Additional Figure 2 Establishment of a cell model of mouse reactive spinal astrocytes.

(A) Primary murine spinal astrocytes were identified via immunocytochemical staining for the astrocyte-specific marker GFAP (green, Alexa Fluor 488). Scale bar: 40 μm . (B) Relative *GFAP* mRNA level in primary murine spinal astrocytes after lipopolysaccharide treatment for 24 hours. The results were normalized by Control group. The data are presented as the mean \pm SEM. The experiments were repeated three times. * $P < 0.05$ (two-tailed Student's t-test). GFAP: Glial fibrillary acidic protein; LPS: lipopolysaccharide.



Additional Figure 3 Localization of neural stem cells in the injured spinal cord of mice.

(A) At 1 week post-injection, immunohistochemical staining showed that FoxJ1⁺ (red, Alexa Fluor 568) cells were localized near the lesion core, with the arrowheads indicating some representative residual neural stem cells and dotted line indicating the lesion core, but there was a distance between FoxJ1⁺ cells and AAVs infected GFP⁺ (green, Alexa Fluor 488) cells (n = 3 mice, four sections per mouse) Scale bar: 50 μ m. (B) Schematics of the location of residual neural stem cells and the injection sites of AAVs after SCI. AAV: Adeno-associated virus; GFP: green fluorescent protein.